

2009

# Temperature-Driven Mixing-Demixing Behavior of Binary Mixtures of the Ionic Liquid Choline Bis(trifluoromethylsulfonyl)imide and Water

Peter Nockeman, *Katholieke Universiteit Leuven*

Koen Binnemans, *Katholieke Universiteit Leuven*

Ben Thijs, *Katholieke Universiteit Leuven*

Tatjana N. Parc-Vogt, *Katholieke Universiteit Leuven*

Klaus Merz, et al.

# Temperature-Driven Mixing-Demixing Behavior of Binary Mixtures of the Ionic Liquid Choline Bis(trifluoromethylsulfonyl)imide and Water

Peter Nockemann,<sup>\*,†</sup> Koen Binnemans,<sup>†</sup> Ben Thijs,<sup>†</sup> Tatjana N. Parac-Vogt,<sup>†</sup> Klaus Merz,<sup>‡</sup> Anja-Verena Mudring,<sup>‡</sup> Preethy Chirukandath Menon,<sup>§</sup> Ravindran Nair Rajesh,<sup>§</sup> George Cordoyiannis,<sup>§</sup> Jan Thoen,<sup>§</sup> Jan Leys,<sup>§</sup> and Christ Glorieux<sup>§</sup>

Department of Chemistry, Laboratory of Coordination Chemistry, Katholieke Universiteit Leuven, Celestijnenlaan 200F, bus 2404, B-3001 Leuven, Belgium, Anorganische Chemie I - Festkörperchemie and Materialien, Ruhr-Universität Bochum, D-44780 Bochum, Germany, and Department of Physics and Astronomy, Laboratory for Acoustics and Thermal Physics, Katholieke Universiteit Leuven, Celestijnenlaan 200D, B-3001 Leuven, Belgium.

Received: October 10, 2008; Revised Manuscript Received: November 18, 2008

The ionic liquid (2-hydroxyethylammonium)trimethylammonium bis(trifluoromethylsulfonyl)imide (choline bistriflimide) was obtained as a supercooled liquid at room temperature (melting point = 30 °C). Crystals of choline bistriflimide suitable for structure determination were grown from the melt in situ on the X-ray diffractometer. The choline cation adopts a folded conformation, whereas the bistriflimide anion exhibits a transoid conformation. The choline cation and the bistriflimide anion are held together by hydrogen bonds between the hydroxyl proton and a sulfonyl oxygen atom. This hydrogen bonding is of importance for the temperature-dependent solubility properties of the ionic liquid. Choline bistriflimide is not miscible with water at room temperature, but forms one phase with water at temperatures above 72 °C (equals upper critical solution temperature). <sup>1</sup>H NMR studies show that the hydrogen bonds between the choline cation and the bistriflimide anion are substantially weakened above this temperature. The thermophysical properties of water-choline bistriflimide binary mixtures were furthermore studied by a photopyroelectric technique and by adiabatic scanning calorimetry (ASC). By photothermal analysis, besides highly accurate values for the thermal conductivity and effusivity of choline bistriflimide at 30 °C, the detailed temperature dependence of both the thermal conductivity and effusivity of the upper and lower part of a critical water-choline bistriflimide mixture in the neighborhood of the mixing-demixing phase transition could be determined with high resolution and accuracy. Together with high resolution ASC data for the heat capacity, experimental values were obtained for the critical exponents  $\alpha$  and  $\beta$ , and for the critical amplitude ratio  $G^+/G^-$ . These three values were found to be consistent with theoretical expectations for a three dimensional Ising-type of critical behavior of binary liquid mixtures.

## Introduction

Although a major amount of physicochemical studies on ionic liquids have so far focused on pure compounds, ionic liquids can also be of great interest as one of the two components of binary liquid mixtures for instance in combination with water. From a technological point of view, the temperature-driven mixing-demixing behavior of many binary mixtures, used as a solvent and chemical reaction medium consisting of the ionic liquid and another liquid, can be exploited under biphasic conditions to perform chemical reactions in the homogeneous phase, and subsequently vary the temperature in order to separate the ionic-liquid-rich phase from the ionic-liquid-lean phase.<sup>1–6</sup> The different affinity of the reaction components and end products to dissolve in one of both physically separated phases then allows to (partially) separate them, making their extraction easier. Thanks to the possibility to design the molecular composition of ionic liquids and to choose the second liquid,

one can tune the differential affinity of particular reaction compounds, for example, by designing an ionic liquid to be hydrophobic, and combining with water, and thus favor the efficiency of the phase (and affiliated compound) separation.

The phase separation behavior of binary liquid mixtures is also interesting in the framework of improving our understanding of critical phenomena. The theory on the critical behavior of phase transitions in general and of fluids and fluid mixtures in particular is nowadays well established.<sup>7,8</sup> Substantial experimental and theoretical progress during the last 40–50 years has resulted in a classification of systems in terms of universality classes.<sup>7–10</sup> In the same universality class, systems have the same set of critical exponents in power laws describing the asymptotic behavior of different properties. For fluids and fluid mixtures the critical behavior of static properties is governed by the 3D Ising universality class. The dynamic critical effects are related to the dynamic universality class of model H.<sup>11</sup>

Experimentally, extensive measurements by high-resolution calorimetric techniques,<sup>12</sup> turbidity and light scattering,<sup>13</sup> and dielectric and refractive index measurements<sup>14</sup> have largely confirmed that consolute points in binary mixtures belong to the 3D Ising universality class. Contrary to static physical properties, transport properties have been much less studied.

\* To whom correspondence should be addressed. E-mail: Peter.Nockemann@chem.kuleuven.be.

<sup>†</sup> Department of Chemistry, Laboratory of Coordination Chemistry, Katholieke Universiteit Leuven.

<sup>‡</sup> Ruhr-Universität Bochum.

<sup>§</sup> Department of Physics and Astronomy, Laboratory for Acoustics and Thermal Physics, Katholieke Universiteit Leuven.

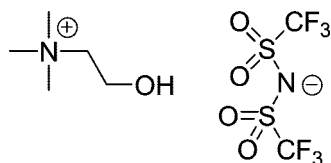


**Figure 1.** Structure of choline bis(trifluoromethylsulfonyl)imide, [choline][Tf<sub>2</sub>N].

Only a limited number of high-resolution results on viscosity, diffusivity, and thermal diffusion have been reported.<sup>15–17</sup> Until very recently conflicting results regarding a critical anomaly for the thermal conductivity,  $\kappa$ , were available in literature. Older data by Filippov and co-workers did not show any evidence for a critical contribution.<sup>18,19</sup> However, more recent work by Mensah-Brown and Wakeham reported a critical anomaly for  $\kappa$  in the binary system butoxyethanol–water.<sup>20,21</sup> Nevertheless, in a high-resolution photopyroelectric study in the beginning of the present decade by some of us, it was shown that the anomaly in butoxyethanol–water is absent as well as in several other binary liquid systems.<sup>22–24</sup> The absence of a critical enhancement in the thermal conductivity at these consolute points are in accordance with theoretical estimates by Anisimov et al. for these (almost) incompressible liquid solutions.<sup>25</sup> Critical binary liquid mixtures involving an ionic liquid have only been very recently considered.<sup>26–36</sup> The study of such systems is important in order to elucidate the impact on the critical behavior of the presence of ionic species in binary liquid mixtures, a role that is less clear. Indeed, several studies on electrolyte systems reported, though contradicted by others, a crossover from 3D Ising to mean field behavior caused by Coulombic interactions.<sup>37</sup> Present consensus assumes this crossover effect is not present since such interactions are absent because the ions are screened off. Thus 3D Ising behavior is expected. This seems to be confirmed recently for the few ionic liquid systems studied.<sup>26,28,29</sup>

In this paper, we report on the thermophysical properties of binary mixtures of water and the ionic liquid choline bis(trifluoromethylsulfonyl)imide (further on abbreviated to choline bistriflimide, [choline][Tf<sub>2</sub>N], Figure 1), determined by means of a photopyroelectric technique and adiabatic scanning calorimetry (ASC). The purpose of this study was to confirm whether 3D Ising behavior is observed for this binary mixture involving an ionic liquid. The thermomorphic behavior was furthermore studied by NMR spectroscopy. Also the optical properties and crystal structure of choline bistriflimide will be discussed.

## Experimental Section

**General Techniques.** The nuclear magnetic resonance (NMR) spectra were recorded on a Bruker Avance 300 spectrometer (operating at 300 MHz for <sup>1</sup>H). DSC traces were measured with a Mettler-Toledo DSC822e module. Coulometric Karl Fischer titrations were made by use of a Mettler Toledo Karl Fischer Titrator model DL39. Absorption spectra were recorded on a Varian Cary 5000 spectrophotometer. Choline chloride was purchased from Acros and lithium bis(trifluoromethylsulfonyl)imide was obtained as a 2 mol L<sup>-1</sup> aqueous solution from IoLiTec.

**Synthesis of Choline Bis(trifluoromethylsulfonyl)imide.** A solution of choline chloride (1 mol, 139.62 g) in 250 mL of water was added under stirring to 500 mL of an aqueous solution of lithium bis(trifluoromethylsulfonyl)imide (1 mol, 287.08 g). The mixture was stirred for 1 h at room temperature and the

aqueous phase separated from the ionic liquid. Lithium chloride formed during the metathesis reaction remained dissolved in the aqueous layer. After separation of the phases, the ionic liquid phase was washed three times with small amounts of water until the silver nitrate test gave negative results. This is an indication that the concentration of remaining chloride impurities is lower than 250 ppm. Finally the ionic liquid has been evaporated to dryness at 120 °C on a rotary evaporator. <sup>1</sup>H NMR (300 MHz, [D<sub>6</sub>]DMSO, TMS):  $\delta$  = 5.29 (t, 1H), 3.84 (m, 2H), 3.39 (m, 2H), 3.10 (s, 9H). <sup>13</sup>C NMR (75.47 MHz, [D<sub>6</sub>]DMSO, TMS):  $\delta$  = 119.5 (CF<sub>3</sub>, q,  $J_{CF}$  = 320 Hz), 67.01 (N–CH<sub>2</sub>), 55.13 (CH<sub>2</sub>), 53.18 (3 × CH<sub>3</sub>). Elemental analysis calcd (%) for C<sub>7</sub>H<sub>14</sub>N<sub>2</sub>O<sub>5</sub>F<sub>6</sub>S<sub>2</sub> ( $M$  = 384.31 g·mol<sup>-1</sup>): C 21.87, H 3.67, N 7.28. Found: C 21.64, H 4.13, N 7.04. Yield: 90%. Mp 30 °C. Density: 1.501 g cm<sup>-3</sup> (35 °C). A water content of 25 ppm was determined using a coulometric Karl Fischer titrator.

**X-ray Crystallography.** Crystals of choline bis(trifluoromethylsulfonyl)imide were grown from the melt in situ on the X-ray diffractometer using the method and experimental setup developed by Boese.<sup>38–41</sup> The method has been successfully used by Winterton et al. to grow crystals of low melting ionic liquids (room-temperature ionic liquids (RTIL)) for X-ray diffraction.<sup>42,43</sup> The liquid was first introduced under inert gas atmosphere into a Lindemann glass capillary (approx 2.5 cm long and 0.3 mm in diameter), sealed, and mounted vertically on a Bruker-AXS-SMART diffractometer in a cold nitrogen stream (Oxford Cryosystem) and subsequently cooled and heated until the compound solidified no longer as a glass but as a polycrystalline material. At this point, the zone-melting technique was applied using the optical heating and crystallization device (OHCD)<sup>44</sup> to grow single crystals. A small section (~1 mm) of the lower portion of the capillary was heated with an IR laser to create a zone of molten material which was slowly moved along the capillary while the laser power was adjusted to sufficiently melt the polycrystalline material. Then the laser beam was moved along the whole capillary from bottom to top in approximately one hour. The laser power was then slowly reduced and the cycles repeated several times until a single crystal of sufficient quality was grown.

After successful single crystal growth, intensity data were collected on a Bruker-axs-SMART diffractometer (MoK $\alpha$  radiation,  $\lambda$  = 0.7170 Å,  $\omega$  scan). The structure was solved by direct methods (SHELXS97) and refined by fullmatrix least-squares against F<sup>2</sup> with all measured reflections (SHELXL97).<sup>45</sup> All non-hydrogen atoms were refined anisotropically and the hydrogen atoms were included riding on the respective parent atom with isotropic thermal displacement factors fixed at at 1.2 times the  $U(\text{eq})$  of the parent atoms (1.5 times for methyl groups). Crystal data: [choline][Tf<sub>2</sub>N], chemical formula C<sub>7</sub>H<sub>14</sub>F<sub>6</sub>N<sub>2</sub>O<sub>5</sub>S<sub>2</sub>, formula weight 384.34 g·mol<sup>-1</sup>, orthorhombic, space group *Pna*2<sub>1</sub> (no. 33),  $a$  = 965.7(5) pm,  $b$  = 1114.1(9) pm,  $c$  = 1465.1(12) pm,  $V$  = 1576(2) × 10<sup>6</sup> pm<sup>3</sup>,  $Z$ ,  $Z$  = 4,  $\rho_{\text{calc}}$  = 1.62 g·cm<sup>-3</sup>,  $T$  = 213(2) K,  $\mu$  = 0.442 mm<sup>-1</sup>,  $F(000)$  = 784; 3876 reflections measured, 2138 unique,  $R_{\text{int}}$  = 0.1280,  $R_1$  = 0.0906,  $wR_2$  = 0.2137 (for reflections  $I > 2\sigma(I)$ ). Crystallographic data (excluding structure factors) for the structure reported in this paper have been deposited with the Cambridge Crystallographic Data Centre as supplementary publication no. CCDC-620456.

**Thermophysical Measurements.** For the photothermal characterization of the binary liquid mixture water–choline bistriflimide, the same approach as in ref 26 has been used. This methodology is conceptually identical to the photopyroelectric (PPE) methods as described in other references,<sup>46–50</sup> but the implementation used is dedicated to the simultaneous determi-

nation of thermal conductivity  $\kappa$  and thermal effusivity  $e$  (using two simultaneous excitation frequencies optimized for good sensitivity to, respectively,  $\kappa$  and  $e$ ) of binary liquid mixtures (dual sensor in, respectively, upper and lower phase). In the configuration used, the measured part of the liquid of interest is sandwiched between a pyroelectric transducer and a cylindrical piston. In the thermal effusivity measuring regime, where the modulation frequency  $f$  is high, so that the thermal diffusion length  $\mu = [\alpha/(\pi f)]^{1/2}$ , with  $\alpha$  the thermal diffusivity of the liquid, is sufficiently smaller than the thickness  $d$  of the liquid layer, the sample layer acts as a virtually semi-infinite thermal impedance for the thermal waves excited and detected in the sensor. In the thermal conductivity regime, where due to the much lower modulation frequency, the thermal waves reach the highly thermally conducting piston, which therefore acts as a heat sink. In this case, the sample layer acts as a thermal barrier between the heated (by modulated LED illumination) sensor and the heat sink, and the value of  $d$  plays a crucial role in the analysis of the data. In our previous work on binary liquids,<sup>22–24</sup> the thickness  $d$  was determined at a reference temperature (at which the binary liquid mixture was mixed) by a calibration measurement in which the sample liquid was replaced by pure water, acting as a reference liquid with known thermal properties. By fitting the frequency dependence of the amplitude and phase (with respect to the illumination) of the signal,  $d$  could be determined. However, due to possible variations of the sensor-heat sink distance (typical variations of the order of 20  $\mu\text{m}$  with respect to a nominal thickness of typically 200  $\mu\text{m}$ ) caused by manipulations of the measurement cell while filling, emptying and refilling the cell with reference and sample liquid, this procedure is likely subject to errors. In our new approach, we make use of an additional, newly developed calibration cell which allows for a very accurate a priori simultaneous determination of the thermal conductivity and thermal effusivity of the sample liquid, and by combining these, its specific heat capacity. The new calibration cell makes use of combined frequency and thickness scans (without a priori knowledge of absolute thicknesses but with precise control of thickness variations) to simultaneously determine the thermal conductivity, the thermal effusivity, and the absolute thickness of the sample. The combined scanning approach lifts the classical fitting degeneracy between the thermal conductivity and the sample thickness in the classically used approach doing a frequency scan at a fixed thickness. Also a third calibration cell, for absolute, accurate determination of the thermal diffusivity of the sample, is now available, allowing to cross-check the  $\kappa$  and  $e$  values. This cell is a user-friendly, fully automated implementation of an approach proposed by Delenclos et al.<sup>51</sup> The resulting availability of very accurate values for all thermal properties of the sample liquid at one or more reference temperatures now allows the calibration of the cell that is used for the high resolution temperature scans, using the sample liquid itself. The calibration is simply done by performing a frequency scan at the reference temperatures and using the known properties of the sample layer to fit the sample thickness. This procedure avoids the use of a reference liquid and the cumbersome manipulations associated with that. Once  $d$  is known, its value can then be used to determine the temperature dependence thermal conductivity of the sample from the amplitude and phase of the photothermal signal during a high resolution temperature scan.

The methodology to determine the temperature dependence of the thermal conductivity and thermal effusivity of binary mixtures has been described in detail in previous work.<sup>22,23</sup> As

mentioned before, the lower and upper part of the mixture essentially fills a gap between a pyroelectric transducer and a gold coated cylindrical piston, acting as a thermal resistance for thermal waves that are optically generated in the transducer. For the thickness determination of the upper and lower sensor, we performed a frequency scan at  $T^{\text{ref}} = 30$  °C. At this temperature, the demixing of the compound is quasi complete, so that we tentatively assumed that the probed sample layer was virtually pure water and pure choline bistriflimide in respectively the upper and lower transducer. Making this assumption, the thickness of the sample in the (heavy) choline bistriflimide-rich phase (lower sensor) was fitted from the frequency scans using the above determined pure choline bistriflimide and water values. The obtained value  $d_{\text{lower}} = (166 \pm 2)$  micron was then retained to extract the varying thermal properties of the lower binary liquid phase from the amplitude and phase of the pyroelectric signal (for details about this iterative procedure see refs 22, 23, and 26 during the whole high-resolution temperature scan, which was performed at a programmed rate of 8 down to 0.2  $\text{mK} \cdot \text{min}^{-1}$  near the transition. In this way, also the thermal conductivity and effusivity were obtained in the mixed phase temperature region. Since the mixed phase has the same composition for both upper and lower sensor, the thermal property values obtained from the lower sensor iteration could be used to calibrate the thickness of the sample in the upper sensor, leading to a value  $d_{\text{upper}} = (148 \pm 4)$  micron. Finally, this value was then used to iteratively determine the varying thermal properties of the sample in the lower sensor in the complete scanned temperature region. With decreasing temperature, the resulting thermal conductivity curve for the water-rich phase asymptotically goes to the value of pure water not far below 30 °C, confirming our earlier assumption.

It is important to mention that for this procedure, the cell gaps were roughly estimated and optimized a priori to the calibration, in order to have a configuration with optimum sensitivity for the thermal properties of interest in the experimentally most favorable frequency range (0.2 Hz for thermal conductivity regime and 1.5 Hz for thermal effusivity regime). The transducers were made of a PZT material with known thermal properties and had a thickness of 520  $\mu\text{m}$  for both upper and lower sensor. Two LEDs were used for upper and lower transducer, each excited with a dual sinusoidal modulation at the frequencies of interest (0.2 and 1.5 Hz). The amplitude and phase of the four pyroelectric current signals were detected by four SR850 lock-in amplifiers of Stanford Research Instruments (SRS) (two lock-in frequencies per sensor signal for upper and lower sensor).

## Results and Discussion

**Synthesis.** A simple metathesis reaction between choline chloride and lithium bis(trifluoromethylsulfonyl)imide ( $\text{LiTf}_2\text{N}$ ) in aqueous solution led to the formation of an RTIL, (2-hydroxyethyl)trimethylammonium bis(trifluoromethylsulfonyl)imide (choline bistriflimide,  $[\text{choline}][\text{Tf}_2\text{N}]$ ) (Figure 1). After the reaction, choline bistriflimide separated spontaneously from the aqueous phase, due to the hydrophobicity of this organic salt. Lithium chloride salt formed during the metathesis reaction remained dissolved in the aqueous layer. This behavior facilitated the purification. After choline bistriflimide was washed several times with water, no chloride impurities could be detected by the silver nitrate test. Choline bistriflimide was dried at 120 °C on a rotary evaporator equipped with a vacuum pump enabling a vacuum up to  $10^{-3}$  mbar. By means of this drying procedure, the water content of the ionic liquid could

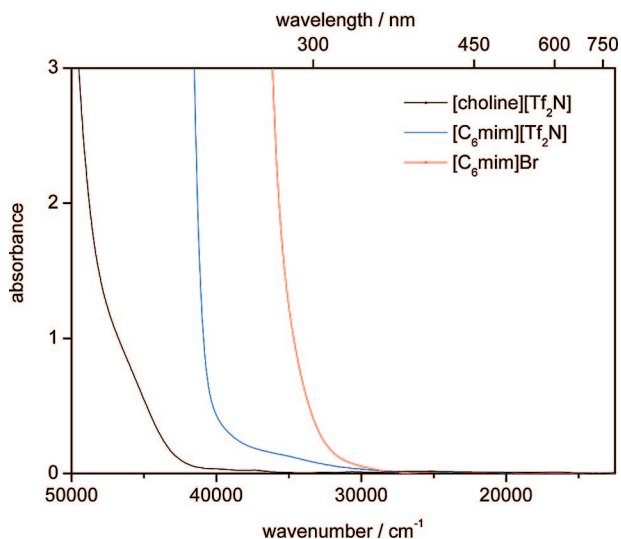


**Figure 2.** Absorption spectrum of choline bis(trifluoromethylsulfonyl)imide (choline bistriflimide) compared to the spectra of 1-hexyl-3-methylimidazolium bis(trifluoromethylsulfonyl)imide ( $[\text{C}_6\text{mim}][\text{Tf}_2\text{N}]$ ) and 1-hexyl-3-methylimidazolium bromide ( $[\text{C}_6\text{mim}][\text{Br}]$ ) at room temperature. The optical path length is 1 cm (quartz cuvette).

be reduced to 25 ppm (determined by coulometric Karl Fischer titration). The ionic liquid choline bistriflimide has already been described earlier.<sup>52</sup> Although choline bistriflimide was obtained as a liquid at room temperature after synthesis, it crystallized out when placed in a freezer ( $-18\text{ }^\circ\text{C}$ ). This indicated that it is a supercooled liquid at room temperature. Study of its thermal behavior by differential scanning calorimetry (DSC) and polarizing optical microscopy (POM) revealed that the compound melts at  $30\text{ }^\circ\text{C}$ , and that solid state polymorphism is present. Between  $3\text{ }^\circ\text{C}$  and the melting point, a plastic crystalline state could be detected. Upon cooling, crystallization was observed at  $-11\text{ }^\circ\text{C}$ . Choline bistriflimide shows a tendency to crystallization rather than to glass formation. This can be ascribed to the low viscosity of the ionic liquid and presumably hydrogen bonding helps to structure the compound even in the liquid state and facilitates crystallization.

**Optical Properties.** Ionic liquids have been applied as solvents for spectroscopic studies.<sup>53–59</sup> Ionic liquids are also being used as a medium for photochemical reactions and for photophysical measurements.<sup>60,61</sup> A high transparency in the visible and ultraviolet spectral region is also desirable for the monitoring of organic reactions by absorption spectroscopy.<sup>62–64</sup> Given the fact that the choline cation contains no aromatic or other conjugated groups, it was expected that choline bistriflimide exhibits no intense absorption bands in the visible and in the ultraviolet spectral region. In addition, the bistriflimide anion has no chromophores. Measurement of the absorption spectrum indeed revealed that the ionic liquid is transparent over a wide optical range.

For the neat choline bistriflimide in a 1 cm quartz cuvette, the absorbance reaches a value of 0.5 at 222 nm, and the UV cutoff is located at about 202 nm. This is in contrast to the well-known imidazolium salts, which often contain colored impurities. Even a carefully purified imidazolium salt is not transparent below 250 nm. In Figure 2, the UV–vis absorption spectrum of choline bistriflimide is compared with that of optically pure 1-hexyl-3-methylimidazolium bistriflimide,  $[\text{C}_6\text{mim}][\text{Tf}_2\text{N}]$ . It is evident from these data that the UV cutoff of choline bistriflimide is about 40 nm lower than that of  $[\text{C}_6\text{mim}][\text{Tf}_2\text{N}]$  and about 75 nm lower than that of  $[\text{C}_6\text{mim}][\text{Br}]$ . Although the absorption spectrum of choline bistriflimide shows

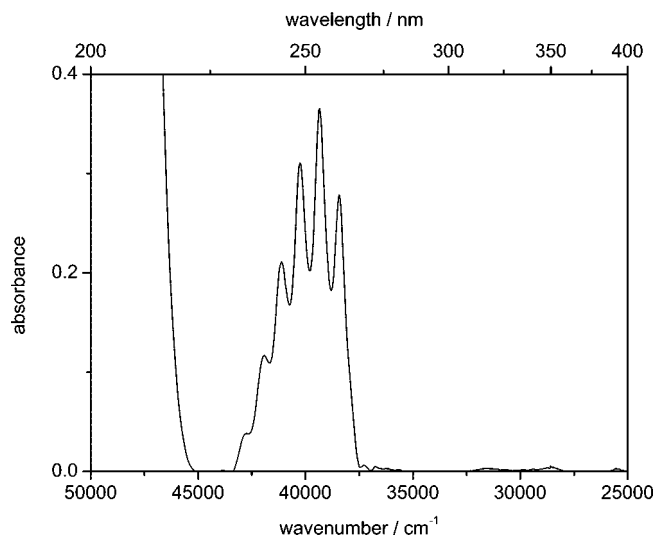


**Figure 3.** Room-temperature absorption spectrum of benzene dissolved in choline bistriflimide.

the tail of an absorption band at wavelengths below 240 nm, this absorption is weak and the absorption band was no longer observed in a spectrum of a compound dissolved in choline bistriflimide when a matching cuvette with choline bistriflimide was placed in the reference beam of the spectrophotometer. In order to illustrate the usefulness of choline bistriflimide as a solvent for spectroscopic studies in the ultraviolet spectral region, the absorption spectrum of a diluted solution of benzene in choline bistriflimide was recorded (Figure 3). The vibrational fine structure of the benzene molecules can clearly be observed.

As a spectrograde solvent, choline bistriflimide is comparable with acetonitrile but has the advantage of being a weakly coordinating solvent and of having a very low volatility (so that spectroscopic studies at high temperature are possible). A drawback of choline bistriflimide is the low solubility of simple inorganic salts in this solvent despite its ionic nature. Choline bistriflimide is closely related to a series of alkoxymethyl(2-hydroxyethyl)dimethylammonium bistriflimide salts prepared by Pernak and co-workers,<sup>65</sup> but in contrast choline bistriflimide can be prepared in a facile one step synthesis by mixing commercially available starting materials.

**Crystal Structure.** Choline bistriflimide crystallizes in the orthorhombic space group  $Pna2_1$  (no. 33) with one cation–anion pair in the asymmetric unit and four ion pairs in the unit cell. The choline cation itself adopts the folded conformation which is commonly found for this cation, the angles are  $\tau(\text{N}-\text{C}-\text{C}-\text{O}) = 63^\circ$  and  $\delta(\text{C}-\text{C}-\text{O}) = 111^\circ$ , respectively.<sup>66–68</sup> In the bistriflimide anion, the  $-\text{CF}_3$  groups adopt a transoid conformation with respect to each other. This conformation is also found for the free acid<sup>69</sup> and is energetically preferred over the cisoid conformation unless packing effects or other intermolecular forces such as complex formation favor the latter one.<sup>70</sup> The choline cation and the bistriflimide anion are held together by hydrogen bonds with an interatomic distance between the hydroxyl proton and the sulfonyl oxygen atom of  $d(\text{O1}\cdots\text{H1}\cdots\text{O21}=\text{S20}) = 205(1)\text{ pm}$  (Figure 4), as the hydrogen electron density has not been localized in the Fourier map and the proton was placed in an idealized position the sulfonyl oxygen and the hydroxyl oxygen interatomic distance of  $d(\text{O1}\cdots\text{O21}) = 284(1)\text{ pm}$  is more meaningful. Both values lie in the expected range for this kind of hydrogen bonding.<sup>71</sup> The molecular structure of choline bistriflimide shows strong similarity to the one of the nonisotypic, nonfluorinated choline

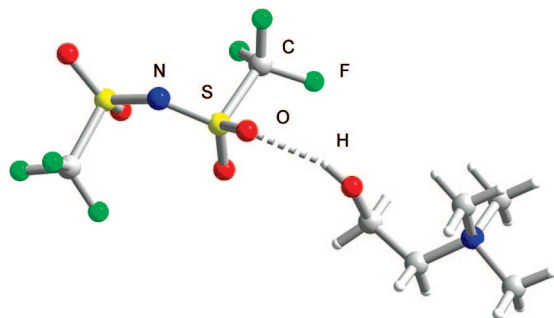


**Figure 4.** View of the crystal structure of [choline][Tf<sub>2</sub>N] approximately along the crystallographic *a*-axis.

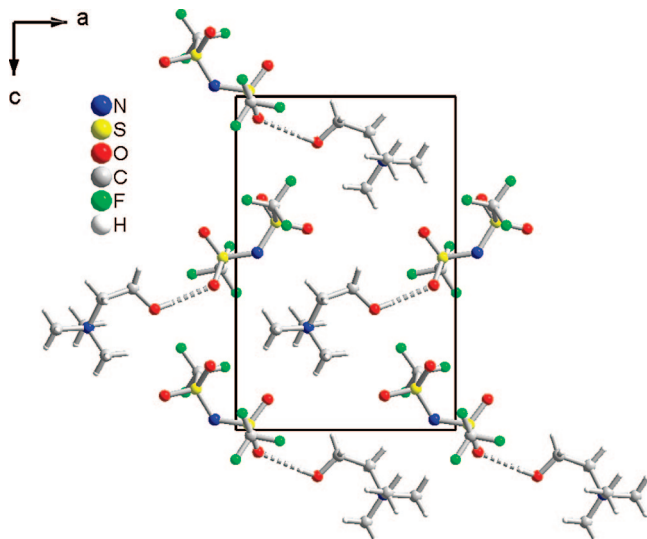


**Figure 5.** View along the crystallographic *b*-axis on a layer of [choline][Tf<sub>2</sub>N]. The hydrogen bonding between the choline cation and the [Tf<sub>2</sub>N]<sup>-</sup> is represented by a dashed line.

dimesylamide (dimesylamide = (CH<sub>3</sub>SO<sub>2</sub>)<sub>2</sub>N<sup>-</sup>).<sup>72</sup> The cation–anion associates are packed in the crystal lattice to layers in the (101) plane (Figure 5).

Significant hydrophobic F⋯F interaction (“fluorine segregation”)<sup>73</sup> as commonly encountered for bis(trifluoromethylsulfonyl)imide structures<sup>74</sup> is also observed for choline bistriflimide. The shortest F⋯F interatomic distances of different –CF<sub>3</sub> groups to each other are found at 330(2) pm for F11 and F12 to F21 and F22, respectively. These contacts connect the above-mentioned layers to a three-dimensional structure. This is in strong contrast to the interactions found in the non-fluorinated compound, where the methyl protons are strongly activated by the –I-effect (electron-withdrawing inductive effect) of the sulfonyl groups so that they participate in the hydrogen bonding network. However, for choline bistriflimide weak –CF<sub>3</sub>⋯H<sub>3</sub>–F hydrogen bonds can be discussed as several F⋯H interatomic contacts below 300 pm are found, some of them as short as 280 pm, with the respective the C⋯F interatomic distances amounting to 326 pm and larger.

**Thermomorphic Behavior.** At room temperature choline bistriflimide forms a two-phase system with water at room temperature with choline bistriflimide in the lower layer. Upon heating a mixture of choline bistriflimide and water, a one-phase system with an upper consolute point at around 72 °C is formed. Cooling of the one-phase mixture results again in phase separation. The phase separation is visually illustrated in Figure 6. The phase diagram of [choline][Tf<sub>2</sub>N]–water (shown in Figure 7) was determined by equilibrating the binary mixture

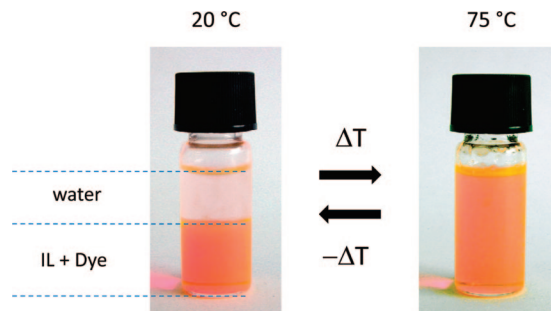


**Figure 6.** Temperature-dependent phase behavior of a binary mixture [choline][Tf<sub>2</sub>N]–water. The ionic liquids phase was dyed with Eosin Y to accentuate the phase boundaries.

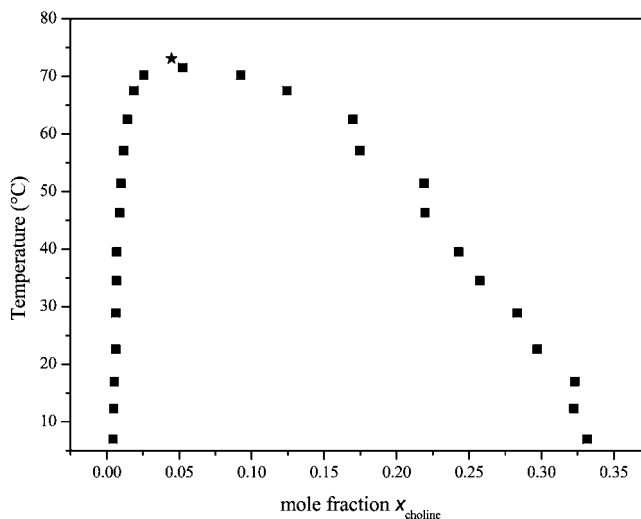
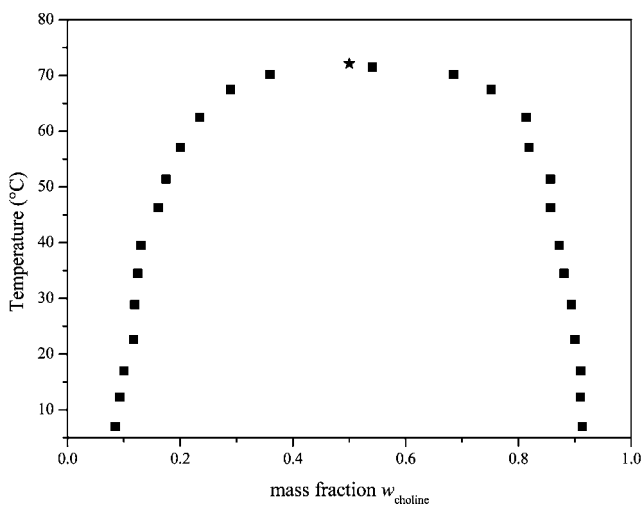


**Figure 7.** The liquid–liquid equilibrium phase diagram (coexistence curve) of the binary mixture [choline][Tf<sub>2</sub>N]–water. The composition of the mixture (expressed via mass fraction of choline bistriflimide,  $w_{\text{choline}}$ , upper part; expressed via mole fraction, lower part) was determined by a gravimetric method. The asterisk denotes the value of concentration derived from fitting of the coexistence curve.

at a given temperature, followed by analysis of the components in the [choline][Tf<sub>2</sub>N] rich phase (lower layer) and in the water-rich phase (upper layer). The composition of the phases was determined by distilling out the water and comparing the original mass with the remaining (nonvolatile) ionic liquid mass. At the critical concentration, the mass fraction of the ionic liquid is 0.524.

To get more insight into the temperature-dependent miscibility of choline bistriflimide with water, we additionally studied a

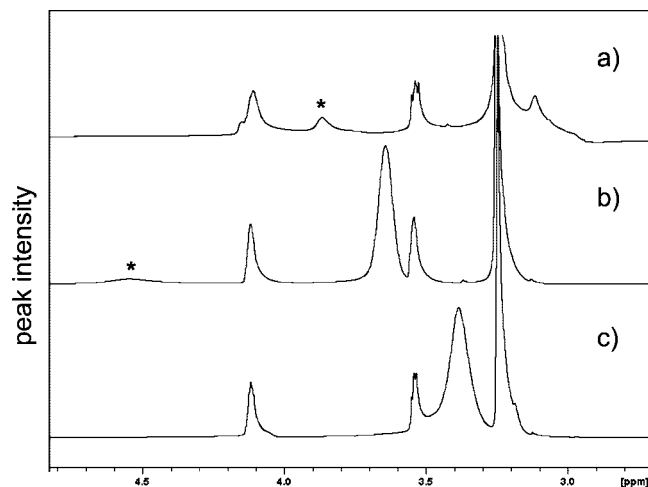


**Figure 8.** Proton NMR spectrum of [choline][Tf<sub>2</sub>N]–water mixture at 25 (a), 70 (b), and 100 °C (c). The hydroxyl resonance (marked with \*) disappears in the one-phase solution at 100 °C.

choline bistriflimide–water mixture by <sup>1</sup>H NMR spectroscopy. Proton NMR spectra of the pure ionic liquid were recorded at 25 and 100 °C, and the only difference observed was sharpening of the peaks as the temperature increased. The integration of four observed resonances at 3.22, 3.58, 4.10, and 3.75, allowed for their unambiguous assignment to three equivalent CH<sub>3</sub> groups, two CH<sub>2</sub> groups, and a hydroxyl proton respectively. <sup>1</sup>H NMR spectra of the [choline][Tf<sub>2</sub>N]–water mixture at room temperature were nearly identical to the spectrum of ionic liquid recorded in the absence of water, indicating the absence of interaction between two phases. The only difference compared to the spectrum of pure ionic liquid was the appearance of a water peak at 3.10 ppm. Heating the sample to 70 °C resulted in shifting and in an intensity increase of H<sub>2</sub>O resonance, consistent with an increase of H<sub>2</sub>O content in the ionic liquid phase with heating. Interestingly, the hydroxyl proton, which at room temperature spectrum could be observed as a well-defined peak, at 70 °C was detected as an extremely broad peak at 4.55 ppm, indicating that upon increase of miscibility with water the hydrogen bonding between hydroxyl proton of choline cation and oxygen atom of the Tf<sub>2</sub>N anion was diminished. When the sample of choline bistriflimide–water was further heated to 100 °C (at which point the one-phase system was fully formed) the hydroxyl resonance completely disappeared, indicating that this proton undergoes fast exchange on the NMR time scale. This implies that the hydrogen bond between anion and cation in [choline][Tf<sub>2</sub>N] is fully broken upon formation of a one-phase system (Figure 8). Analogous behavior was observed for other ionic liquid studied in our laboratory in which proton NMR spectra indicated loss of hydrogen bonding upon formation of a one-phase system with water.<sup>26</sup>

**Thermophysical Measurements.** In view of characterizing the second order phase transition via the thermal parameters  $\kappa$ ,  $e$  (photothermal experiments), and  $c$  (adiabatic scanning calorimetry (ASC) experiment) as good as possible, mixtures were prepared at the critical concentration, which was interpolated from the data in Figure 9 being  $w_{\text{choline}} = 0.524$  and  $w_{\text{water}} = 0.476$  for choline bistriflimide and water, respectively (expressed in mass fractions). At the time when these experiments have been performed, our absolute calibration cell for, respectively, ( $\kappa$ ,  $e$ ) determination was only operational at room temperature, so that we could not determine the thermal properties of the binary mixture to 85 °C, well above the mixing point at 72.10 °C in the mixed phase.

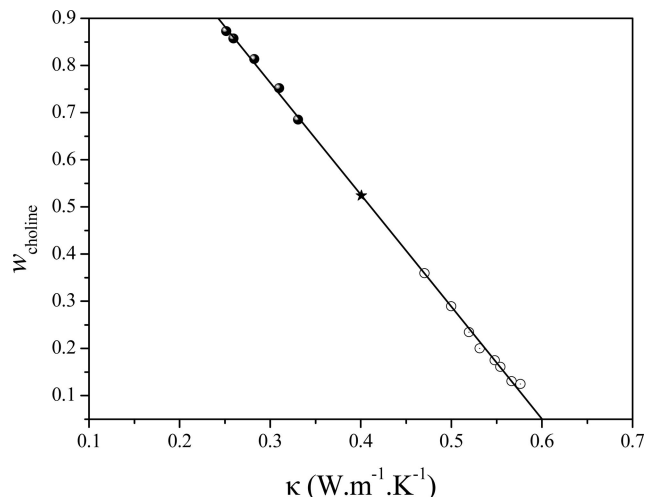


**Figure 9.** Experimental datapoints (circles) and linear fit (line) for the relation between the phase composition (expressed by  $w_{\text{choline}}$  as obtained from Figure 7) and the thermal conductivity  $\kappa$  (data obtained from photopyroelectric measurements). The correlation was obtained by pairing experimental  $w_{\text{choline}}$  or  $w_{\text{water}} = 1 - w_{\text{choline}}$  and  $\kappa$  values for a choline bistriflimide–water mixture at different temperatures in the choline bistriflimide-rich phase (solid symbols) and choline bistriflimide-poor phase (open symbols). In the neighborhood of the critical concentration data points are missing because of the limited resolution in the  $w_{\text{choline}}(T)$  curve. The asterisk denotes the value of critical conductivity derived from the linear fit.

However, from combined thickness and frequency scans with the two calibration cells we determined the values at 30 °C of pure choline bistriflimide at  $\kappa = (0.26 \pm 0.01) \text{ W} \cdot \text{m}^{-1} \cdot \text{K}^{-1}$  and  $e = (660 \pm 3) \text{ J} \cdot \text{m}^{-2} \cdot \text{K}^{-1} \cdot \text{s}^{-1/2}$ . Statistical analysis of the fitting parameter dependence of the  $\chi^2$  value allowed to determine the above given uncertainty on the retrieved sample parameters, both without (variance determination using least-squares approach) and with (variance and covariance determination using the most squares approach) taking into account the covariance between fitting parameters. By combination we derived from the  $\kappa$  and  $e$  values also the heat capacity quantities  $\rho c = e^2/\kappa = (1.71 \pm 0.07) \times 10^6 \text{ J} \cdot \text{m}^{-1} \cdot \text{K}^{-1}$  and  $c = (1140 \pm 50) \text{ J} \cdot \text{kg}^{-1} \cdot \text{K}^{-1}$  (the density of choline bistriflimide at room temperature was obtained by pycnometry as  $\rho = (1501 \pm 8) \text{ kg} \cdot \text{m}^{-3}$  and the thermal diffusivity  $\alpha = \kappa^2/e^2 = (1.55 \pm 0.12) \times 10^{-7} \text{ m}^2 \cdot \text{s}^{-1}$ ). All results are tabulated in Table 1. The accuracy of both calibration cells has been validated by comparing (see Table 2) resulting values of water at 25 °C:  $K = (0.600 \pm 0.002) \text{ W} \cdot \text{m}^{-1} \cdot \text{K}^{-1}$ ,  $e = (1589 \pm 2) \text{ J} \cdot \text{m}^{-2} \cdot \text{K}^{-1} \cdot \text{s}^{-1/2}$ ,  $\rho c = e^2/\kappa = 4.19 \pm 0.02) \times 10^6 \text{ J} \cdot \text{m}^{-1} \cdot \text{K}^{-1}$ ,  $\alpha = \kappa^2/e^2 = (1.426 \pm 0.007) \times 10^{-7} \text{ m}^2 \cdot \text{s}^{-1}$  with literature values.<sup>75</sup>

The  $\kappa$ -curves in the upper and lower phase show the behavior that is expected from the mass fractions  $w_1(T)$  and  $w_2(T)$ , that is, linear and coincident (order parameter  $S = \Delta w = w_2 - w_1 = 0$ ) in the mixed phase, and with  $\Delta w(T)$  following a power law<sup>7–9</sup> in the two-phase region

$$\Delta w_{\text{two-phase}}(T) = C_{\text{two-phase}}(T) = A + BT + D \left( \frac{T_c - T}{T_c} \right)^\beta \quad (1)$$

with  $T_c$  the critical temperature,  $\beta$  the critical exponent, and  $D$  the critical amplitude. The assumption that for this mixture the thermal conductivity is a good measure for the mass fraction is proven in Figure 9, where the thermal conductivities of the upper

**TABLE 1: Comparison between Fitting Results and Literature Values for Thermal Properties of Water at 25 °C**

	result from fit of amplitude frequency scan	result from fit of phase frequency scan	result from fit of complex frequency scan	literature value	unit
thermal conductivity	0.602 ± 0.002	0.597 ± 0.002	0.600 ± 0.002	0.598 <sup>a</sup> 0.66 ± 0.07 <sup>c</sup>	W·m <sup>-1</sup> ·K <sup>-1</sup>
thermal effusivity	1588 ± 1	1589 ± 3	1589 ± 2	1589 <sup>a</sup> 1582 <sup>b</sup> 1555 <sup>c</sup>	J·m <sup>-2</sup> ·K <sup>-1</sup> ·s <sup>-1/2</sup>
offset thickness	45.3 ± 0.3	44.3 ± 0.7	44.0 ± 0.4		μm
specific heat capacity	4.20 ± 0.01 <sup>d</sup>	4.24 ± 0.02 <sup>d</sup>	4.22 ± 0.02 <sup>d</sup>	4.181 <sup>a</sup> 4.1 ± 0.1 <sup>c</sup>	kJ·kg <sup>-1</sup> ·K <sup>-1</sup>
thermal diffusivity	1.437 ± 0.007 <sup>d</sup>	1.411 ± 0.008 <sup>d</sup>	1.426 ± 0.008 <sup>d</sup>	1.430 <sup>b</sup>	10 <sup>-7</sup> m <sup>2</sup> ·s <sup>-1</sup>

<sup>a</sup> Direct or derived properties according to tabulated data in ref 75 at  $T = 25$  °C. <sup>b</sup> According to ref 81 at room temperature. <sup>c</sup> According to ref 49 at room temperature. <sup>d</sup> Our specific heat capacity and thermal diffusivity were extracted from the values of  $\kappa$  and  $e$  via the relations  $C = e^2/(\rho\kappa)$  and  $\alpha = \kappa^2/e^2$  with  $\rho = 997$  kg·m<sup>-3</sup> at  $T = 25$  °C.<sup>82</sup>

**TABLE 2: Comparison between Fitting Results for Thermal Properties of Choline Bistriflimide at 30 °C**

	result from fit of amplitude frequency scan	result from fit of phase frequency scan	result from fit of complex frequency scan	unit
thermal conductivity	0.26 ± 0.01	0.26 ± 0.01	0.26 ± 0.01	W·m <sup>-1</sup> ·K <sup>-1</sup>
thermal effusivity	672 ± 3	660 ± 3	663 ± 3	J·m <sup>-2</sup> ·K <sup>-1</sup> ·s <sup>-1/2</sup>
offset thickness	57 ± 1	56.7 ± 0.4	57 ± 1	μm
specific heat capacity	1.15 ± 0.05 <sup>a</sup>	1.12 ± 0.04 <sup>a</sup>	1.13 ± 0.04 <sup>a</sup>	kJ·kg <sup>-1</sup> ·K <sup>-1</sup>
thermal diffusivity	1.50 ± 0.08 <sup>a</sup>	1.55 ± 0.09 <sup>a</sup>	1.54 ± 0.09 <sup>a</sup>	10 <sup>-7</sup> m <sup>2</sup> ·s <sup>-1</sup>

<sup>a</sup> Our specific heat capacity and thermal diffusivity were extracted from the values of  $\kappa$  and  $e$  via the relations  $C = e^2/(\rho\kappa)$   $\alpha = \kappa^2/e^2$  with  $\rho = (1501 \pm 8)$  kg·m<sup>-3</sup> determined by pycnometry.

and lower phase show a linear relation with the directly measured mass fractions of the respective phases for different temperatures, determined as described above. Exploiting this relation, we have fitted the thermal conductivity difference  $\Delta\kappa$  according to eq 1, leaving  $A$ ,  $B$ ,  $D$ , and  $\beta$  as free-fitting parameters while fixing the value for  $T_c$  at 71.28 °C (value based on visual estimate). The corresponding statistical analysis for  $\beta$  has shown that both the  $\chi^2$  function (sum of quadratic residues between experimental data and theoretical fit versus  $\beta$  with other fitting parameters fixed) and the most squared function (sum of quadratic residues between experimental data and theoretical fit versus  $\beta$  while looking for the best fitting set of other parameters for every  $\beta$  value) go through a parabolic minimum at  $(0.323 \pm 0.001)$ , which is very close to the theoretical 3D Ising value of  $\beta = 0.326$ ,<sup>76,77</sup> strengthening our conclusion of 3D Ising behavior.

The log–log plot of normalized thermal conductivity difference  $\Delta\kappa/\kappa_{\text{ref}}$  (with  $\kappa_{\text{ref}}$  the thermal conductivity of the mixed phase right above the critical point) between the water-rich and choline bistriflimide-rich phase as in Figure 10, confirms order parameter like power law behavior with critical exponent  $\beta$  around 0.326.

By using a dual modulation frequency for the LED excitation of both upper and lower sensor and dual lock-in detection for each sensor signal, experimental data for the thermal effusivity (Figure 11) also could be obtained simultaneously with the thermal conductivity values in Figure 12. In the mixed phase above  $T_c = 72.10$  °C, the curves are coincident. The dotted line is the average of both curves. As in Figure 12, the jump at  $T_c$  reveals that the composition of the sample mixture was not exactly equal to the critical value. The thermal effusivity behavior contains both the critical behavior of the thermal conductivity and of the heat capacity. However, the anomaly of the latter quantity is too small to be reliably extracted from the relation  $(\rho c)(T) = e(T)^2/\kappa(T)$ .

In Figure 13, the specific heat capacity  $c_{\text{tot}}(T)$  of the total sample, determined by high resolution adiabatic scanning calorimetry,<sup>78</sup>

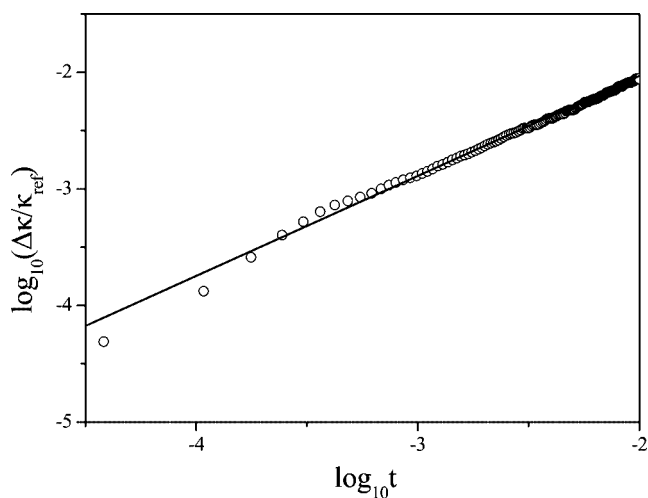


**Figure 10.** Log–log plot of the critical power law behavior of experimental data (circles) for the normalized thermal conductivity difference  $\Delta\kappa/\kappa_{\text{ref}}$  (with  $\kappa_{\text{ref}}$  the thermal conductivity of the mixed phase right above the critical point) between the water-rich and choline bistriflimide-rich phase. Under the assumption (validated in Figure 9) that the thermal conductivity is proportional with the concentration, the plotted quantity should reflect the critical behavior of the order parameter. This is confirmed by the quasi-linear behavior (indicated by linear fit (line)) with slope very close to the critical exponent  $\beta = 0.326$ .

which is a method that is perfectly dedicated for the analysis of critical behavior of the heat capacity at phase transitions, is shown. The amplitude of the specific heat divergence is small with respect to other compounds. Following two-scale-factor universality,<sup>79</sup> this would result in a large amplitude for the correlation length anomaly. However, as far as we know, no turbidity data for choline bistriflimide–water that could elucidate this are available in literature. At this second order phase transition of 3D Ising type,  $c_1(T)$  and  $c_2(T)$  are expected to diverge as  $c(T) = E + FT + G^\pm |(T_c - T)/(T_c)|^{-\alpha} \equiv E + FT + G^\pm t^{-\alpha}$  ( $t$  is the reduced temperature)

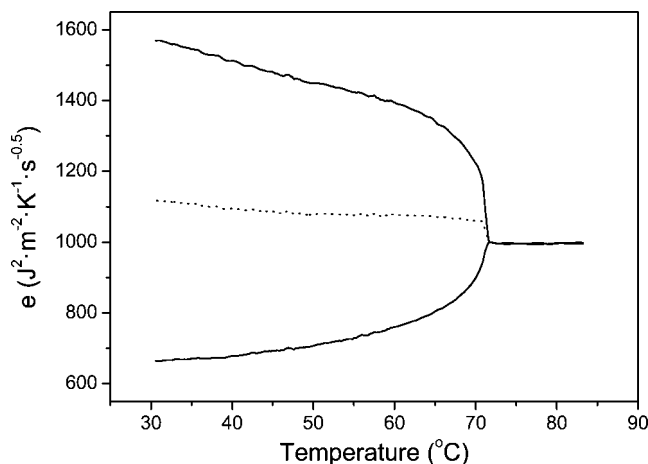


**Figure 11.** Temperature dependence of the thermal effusivity of a choline bistriflimide–water mixture measured by the upper sensor (water-rich phase, upper full curve) and lower (choline bistriflimide-rich phase, lower full curve) sensor during a cooling scan starting in the mixed phase. By using a dual modulation frequency for the LED excitation of both upper and lower sensor and dual lock-in detection for each sensor signal, the experimental data could be obtained simultaneously with the thermal conductivity values in Figure 12. In the mixed phase above  $T_c = 72.10$  °C, the curves are coincident. The dotted line is the average of both curves. As in Figure 12, the jump at  $T_c$  reveals that the composition is not exactly the critical one. The thermal effusivity behavior contains both the critical behavior of the thermal conductivity and of the heat capacity. However, the anomaly of the latter quantity is too small to be reliably extracted from the relation  $(\rho c)(T) = e(T)^2/\kappa(T)$ .

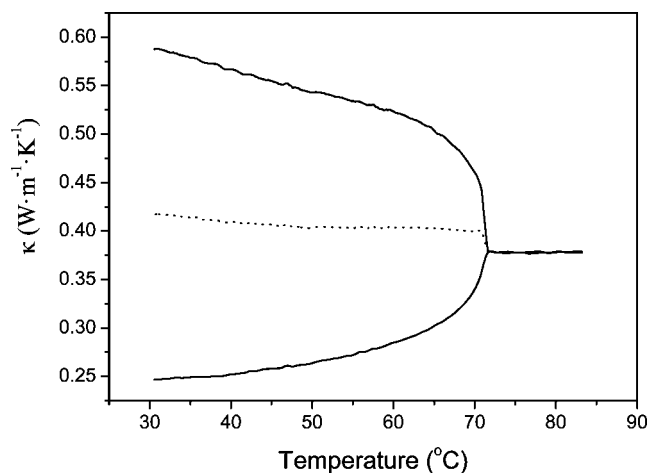


**Figure 12.** Temperature dependence of the thermal conductivity of a choline bistriflimide–water mixture measured by the upper sensor (water-rich phase, upper full curve) and lower (choline bistriflimide-rich phase, lower full curve) sensor. In the mixed phase above  $T_c = 72.10$  °C, the curves are coincident. The dotted line is the average of both curves. The jump at  $T_c$  reveals that the composition of the sample mixture was not exactly equal to the critical value. This only has some impact on the dependence close to  $T_c$ . As previously reported for other binary mixtures<sup>22–24</sup> within the experimental error bar there is no critical anomaly in the thermal conductivity behavior around  $T_c$ .

with a 3D Ising value for the critical exponent  $\alpha = 0.110$ ,<sup>76</sup> and  $G^\pm$  is the critical amplitude respectively above and below  $T_c$ . The good correspondence of the best fit in Figure 13 with the critical exponent value fixed to  $\alpha = 0.110$ <sup>76</sup> and with the optimization of the fitting constants  $E$ ,  $F$ ,  $T_c$ , and  $G^\pm$ ,  $\alpha$  confirms consistence of the experimental data with theoretical predictions for 3D Ising behavior. Also the ratio of the critical amplitudes  $G^+/G^- = (0.54 \pm 0.07)$  is consistent with the theoretical value  $G^+/G^- = 0.54$ .<sup>80</sup> The critical temperature determined from ASC was found to be  $T_c = (72.10 \pm 0.02)$  °C.

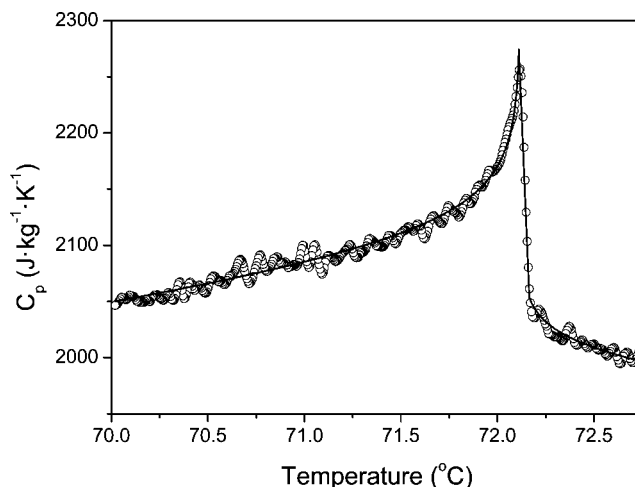


**Figure 13.** Experimental ASC data (circles) for the critical behavior of the specific heat capacity of a critical choline bistriflimide–water mixture. The critical anomaly is relatively small but can be clearly resolved. The full line reflects the best theoretical fit with of the critical exponent fixed to the theoretical value  $\alpha = 0.110$  and all other model parameters left free. Also the ratio between the critical amplitudes  $A^+/A^- = (0.54 \pm 0.07)$  is consistent with the theoretically predicted value 0.54.<sup>76,77,80</sup>

## Conclusions

The ionic liquid choline bistriflimide shows a marked temperature dependent miscibility with water. At room temperature, this ionic liquid is not miscible with water, but above 72.10 °C a one-phase system is formed. This illustrates that one should use the terms “hydrophobic ionic liquid” and “hydrophilic ionic liquid” with caution. By photothermal analysis, besides highly accurate values for the thermal conductivity, the thermal effusivity and the thermal diffusivity of choline bistriflimide at 30 °C, the detailed temperature dependence of both the thermal conductivity, and effusivity of the upper and lower part of a critical choline bistriflimide–water mixture in the neighborhood of the mixing-demixing phase transition could be determined with high resolution and accuracy.

Together with high resolution ASC data for the heat capacity, the critical behavior was found to be consistent with theoretical expectations for power law behavior with critical exponents  $\alpha$  and  $\beta$ . Moreover, the fitting result for the critical amplitude ratio  $G^+/G^-$  was consistent with theoretically predicted values in the case of 3D Ising-type critical behavior of binary liquid mixtures.

**Acknowledgment.** This project was supported by the F.W.O.-Flanders (Projects G.0117.03 and G.0125.03) and by the K.U.Leuven (Projects GOA 08/05, GOA 2002/04 and IDO/05/005). The authors gratefully acknowledge the financial support of the DFG priority program SPP 1191 “Ionic Liquids” and wish to thank IoLiTec (Denzlingen, Germany) for support of the ionic liquid research.

**Supporting Information Available:** CIF file of the crystal structure. This material is available free of charge via the Internet at <http://pubs.acs.org>.

## References and Notes

- (1) Welton, T. *Chem. Rev.* **1999**, *99*, 2071–2083.
- (2) Wasserscheid, P.; Keim, W. *Angew. Chem., Int. Ed.* **2000**, *39*, 3773–3789.
- (3) Dupont, J.; de Souza, R. F.; Suarez, P. A. Z. *Chem. Rev.* **2002**, *102*, 3667–3691.
- (4) Sheldon, R. *Chem. Commun.* **2001**, 2399–2407.
- (5) Parvulescu, V. I.; Hardacre, C. *Chem. Rev.* **2007**, *107*, 2615–2665.

- (6) Plechkova, N. V.; Seddon, K. R. *Chem. Soc. Rev.* **2008**, *37*, 123–150.
- (7) Anisimov, M. A. *Critical Phenomena in Liquids and Liquid Crystals*; Gordon and Breach: Philadelphia, 1990.
- (8) Anisimov, M. A.; Sengers, J. V. In *Critical and Crossover Phenomena in Fluids and Fluid Mixtures, Supercritical Fluids—Fundamentals and Applications*; Kiran, E., Debenedetti, P. G., Peters C. J., Eds.; Kluwer: Dordrecht, 2000; pp 89–121.
- (9) Binney, J. J.; Dowrick, N. J.; Fisher, A. J.; Newman, M. E. J. *The Theory of Critical Phenomena*; Clarendon: London, 1992.
- (10) Chaikin, P. M.; Lubenski, T. C. *Principles of Condensed Matter Physics*; University Press: Cambridge, 1995.
- (11) Siggia, E. D.; Halperin, B. I.; Hohenberg, P. C. *Phys. Rev. B* **1976**, *13*, 2110–2123.
- (12) Thoen, J.; Hamelin, J.; Bose, T. K. *Phys. Rev. E* **1996**, *53*, 6264–6270, and references cited therein.
- (13) Müller, O.; Winkelmann, J. *Phys. Rev. E* **1999**, *59*, 2026–2038.
- (14) Thoen, J.; Bose, T. K. In *Handbook of Low and High Dielectric Constant Materials and Their Applications*; Nalwa, H. S., Ed.; Academic Press, New York, 1999; pp 501–561.
- (15) Berg, R.; Moldover, M. J. *Chem. Phys.* **1988**, *89*, 3694–3704.
- (16) Zielesny, A.; Schmitz, J.; Limberg, S.; Aizpiri, A. G.; Fusenýg, S.; Woermann, D. *Int. J. Thermophys.* **1994**, *15*, 67–94.
- (17) Wiegand, S.; Köhler, W. In *Thermal Nonequilibrium Phenomena in Fluid Mixtures, Lecture Notes in Physics*; Köhler, W., Wiegand, S., Eds.; Springer: Berlin, 2002; Vol. 584, pp 181–210.
- (18) Gerts, I. G.; Filippov, L. P. *Zh. Fiz. Khim.* **1956**, *30*, 2424–2428.
- (19) Filippov, L. P. *Int. J. Heat Mass Transfer* **1968**, *11*, 331–345.
- (20) Mensah-Brown, H.; Wakeham, W. A. *Int. J. Thermophys.* **1994**, *15*, 647–659.
- (21) Mensah-Brown, H.; Wakeham, W. A. *Int. J. Thermophys.* **1995**, *16*, 237–244.
- (22) Pittois, S.; Van Roie, B.; Glorieux, C.; Thoen, J. *J. Chem. Phys.* **2004**, *121*, 1866–1872.
- (23) Pittois, S.; Van Roie, B.; Glorieux, C.; Thoen, J. *J. Chem. Phys.* **2005**, *122*, 24504(1–7)
- (24) Pittois, S.; Sinha, G. P.; Glorieux, C.; Thoen, J. Proceedings of the 27th International Thermal Conductivity Conference and 15th International Thermal Expansion Symposium, Knoxville, TN, October 26–29, 2003; DEStech Publications: Lancaster, PA, 2004; pp 164–173.
- (25) Anisimov, M. A.; Gorodetskii, E. E.; Kulikov, V. D.; Povodyrev, A. A.; Sengers, J. V. *Physica A* **1995**, *220*, 277–324.
- (26) Nockemann, P.; Thijs, B.; Pittois, S.; Thoen, J.; Glorieux, C.; Van Hecke, K.; Van Meervelt, L.; Kirchner, B.; Binnemans, K. *J. Phys. Chem. B* **2006**, *110*, 20978–20992.
- (27) Schröer, W.; Wagner, A.; Stanga, O. *J. Mol. Liq.* **2006**, *127*, 2–9.
- (28) Wagner, M.; Stanga, O.; Schröer, W. *Phys. Chem. Chem. Phys.* **2004**, *6*, 4421–4431.
- (29) Schröer, W. In *Ionic soft matter. Modern trends and applications*; NATO Science Series II: Mathematics, Physics and Chemistry; Henderson, D., Holovko, M., Trokhymchuk, A., Eds.; Springer: Berlin, 2005; Vol. 206, pp 143–180.
- (30) Saracsan, D.; Rybarsch, C.; Schröer, W. *Z. Phys. Chem.* **2006**, *220*, 1417–1437.
- (31) Schröer, W. *J. Mol. Liq.* **2006**, *125*, 164–173.
- (32) Lachwa, J.; Szydłowski, J.; Makowska, A.; Seddon, K. R.; Esperanca, J. M. S. S.; Guedes, H. J. R.; Rebelo, L. P. N. *Green Chem.* **2006**, *8*, 262–267.
- (33) Rebelo, L. P. N.; Najdanovic-Visak, V.; Visak, Z. P.; da Ponte, M. N.; Szydłowski, J.; Cerdeirina, C. A.; Troncoso, J.; Romani, L.; Esperanca, J.; Guedes, H. J. R.; de Sousa, H. C. *Green Chem.* **2004**, *6*, 369–381.
- (34) Crosthwaite, J. M.; Aki, S. N. V. K.; Maginn, E. J.; Brennecke, J. F. *J. Phys. Chem. B* **2004**, *108*, 5113–5119.
- (35) Crosthwaite, J. M.; Muldoon, M. J.; Aki, S.N.V.K.; Maginn, E. J.; Brennecke, J. F. *J. Phys. Chem. B* **2006**, *110*, 9354–9361.
- (36) Butka, A.; Vale, V. R.; Saracsan, D.; Rybarsch, C.; Weis, V. C.; Schröer, W. *Pure Appl. Phys.* **2008**, *80*, 1613–1630.
- (37) Gutkowski, K. I.; Anisimov, M. A.; Sengers, J. V. *J. Chem. Phys.* **2001**, *114*, 3133–3148.
- (38) Kirchner, M. T.; Boese, R.; Billups, W. E.; Norman, L. R. *J. Am. Chem. Soc.* **2004**, *126*, 9407–9412.
- (39) Thalladi, V. R.; Brasselet, S.; Weiss, H.-C.; Blaser, D.; Katz, A. K.; Carrell, H. L.; Boese, R.; Zyss, J.; Nangia, A.; Desiraju, G. R. *J. Am. Chem. Soc.* **1998**, *120*, 2563–2577.
- (40) Boese, R.; Weiss, H. C.; Blaser, D. *Angew. Chem., Int. Ed.* **1999**, *38*, 988–992.
- (41) Boese, R.; Kirchner, M. T.; Billups, W. E.; Norman, L. R. *Angew. Chem., Int. Ed.* **2003**, *42*, 1961–1963.
- (42) Choudhury, A. R.; Winterton, N.; Steiner, A.; Cooper, A. I.; Johnson, K. A. *J. Am. Chem. Soc.* **2005**, *127*, 16792–16793.
- (43) Choudhury, A. R.; Winterton, N.; Steiner, A.; Cooper, A. I.; Johnson, K. A. *CrystEngComm* **2006**, *8*, 742–745.
- (44) Optical Heating & Crystallization Device, <http://www.ohcd-system.com>.
- (45) *SHELXTL-PC*, Manual Version 5.1; Bruker Analytical X-ray Systems Inc.: Madison, WI, 1997.
- (46) Matvienko, A.; Mandelis, A. *Rev. Sci. Instrum.* **2005**, *76*, 104901.
- (47) Matvienko, A.; Mandelis, A. *Rev. Sci. Instrum.* **2006**, *77*, 064906.
- (48) Pittois, S.; Chirtoc, M.; Glorieux, C.; Van den Bril, W.; Thoen, J. *Anal. Sci.* **2001**, *17*, s110–s113.
- (49) Caerels, J.; Glorieux, C.; Thoen, J. *Rev. Sci. Instrum.* **1998**, *69*, 2452–2458.
- (50) Caerels, J.; Glorieux, C.; Thoen, J. *Rev. Sci. Instrum.* **2000**, *71*, 1–7.
- (51) Delenclos, S.; Dadarlat, D.; Houriez, N.; Longuemart, S.; Kolinsky, C.; Hadj Sahraoui, A. *Rev. Sci. Instrum.* **2007**, *78*, 024902024902–5.
- (52) Couling, D. J.; Bernot, R. J.; Docherty, K. M.; Dixon, J. K.; Maginn, E. J. *Green Chem.* **2006**, *8*, 82–90.
- (53) Puntus, L. N.; Schenk, K. J.; Bünzli, J.-C. G. *Eur. J. Inorg. Chem.* **2005**, *473*, 9–4744.
- (54) Guillet, E.; Imbert, D.; Scopelliti, R.; Bünzli, J.-C. G. *Chem. Mater.* **2004**, *16*, 4063–4070.
- (55) Driesen, K.; Nockemann, P.; Binnemans, K. *Chem. Phys. Lett.* **2004**, *395*, 306–310.
- (56) Nockemann, P.; Beurer, E.; Driesen, K.; Van Deun, R.; Van Hecke, K.; Van Meervelt, L.; Binnemans, K. *Chem. Commun.* **2005**, 4354–4356.
- (57) Arenz, S.; Babai, A.; Binnemans, K.; Driesen, K.; Giernoth, R.; Mudring, A. V.; Nockemann, P. *Chem. Phys. Lett.* **2005**, *402*, 75–79.
- (58) Samikkanu, S.; Mellem, K.; Berry, M.; May, P. S. *Inorg. Chem.* **2007**, *46*, 7121–7128.
- (59) Nockemann, P.; Binnemans, K.; Driesen, K. *Chem. Phys. Lett.* **2005**, *415*, 131–136.
- (60) Álvaro, M.; Carbonell, E.; Ferrer, B.; García, H.; Herance, J. R. *Photochem. Photobiol.* **2006**, *82*, 185–190.
- (61) Karmakar, R.; Samanta, A. *J. Phys. Chem.* **2003**, *A107*, 7340–7346.
- (62) Lancaster, N. L.; Welton, T.; Young, G. B. *J. Chem. Soc., Perkin Trans.* **2001**, *2*, 2267–2270.
- (63) Skrzypczak, A.; Neta, P. *Int. J. Chem. Kinet.* **2004**, *25*, 3–258.
- (64) Crowhurst, L.; Lancaster, N. L.; Pérez Arlandis, J. M.; Welton, T. *J. Am. Chem. Soc.* **2004**, *126*, 11549–11555.
- (65) Pernak, J.; Chwała, P.; Syguda, A. *Pol. J. Chem.* **2004**, *78*, 539–546.
- (66) Frydenvang, K.; Jensen, B.; Nielsen, K. *Acta Cryst. C* **1992**, *48*, 1343–1345.
- (67) Frydenvang, K.; Hjelvang, G.; Jensen, B.; Dorosario, S. M. M. *Acta Cryst. C* **1994**, *50*, 617–623.
- (68) Nockemann, P.; Thijs, B.; Driesen, K.; Janssen, C. R.; Van Hecke, K.; Van Meervelt, L.; Kossmann, S.; Kirchner, B.; Binnemans, K. *J. Phys. Chem. B* **2007**, *111*, 5254–5263.
- (69) Haas, A.; Klare, C.; Betz, P.; Bruckmann, J.; Kruger, C.; Tsay, Y.-H.; Aubke, F. *Inorg. Chem.* **1996**, *35*, 1918–1925.
- (70) Mudring, A. V.; Babai, A.; Arenz, S.; Giernoth, R. *Angew. Chem., Int. Ed.* **2005**, *44*, 5485–5488.
- (71) Steiner, T. *Acta Crystallogr. B* **1998**, *54*, 456–463.
- (72) Henschel, D.; Moers, O.; Wijaya, K.; Wirth, A.; Blaschette, A.; Jones, P. G. *Z. Naturforsch., B: Chem. Sci.* **2002**, *57*, 534–536.
- (73) Reichenbacher, K.; Süß, H. I.; Hulliger, J. *Chem. Soc. Rev.* **2005**, *34*, 22–30.
- (74) Babai, A.; Mudring, A.-V. *Inorg. Chem.* **2006**, *45*, 3249–3255.
- (75) Grigull, U.; Sander, H. *Wärmeleitung*; Springer: Berlin, 1990.
- (76) Zinn-Justin, J. *Phys. Rep.* **2001**, *344*, 159–178.
- (77) Wang, J.; Cerdeirina, C. A.; Anisimov, M. A.; Sengers, J. V. *Phys. Rev. E* **2008**, *77*, 031127-1–031127-12.
- (78) Thoen, J. In *Physical Properties of Liquid Crystals*; Demus, D., Goodby, J., Gray, G., Spiess, H.-W., Vill, V., Eds.; Wiley-VCH: Weinheim, 1997; pp 208–232.
- (79) Privman, V.; Hohenberg, P. C.; Aharony, A. In *Phase Transitions and Critical Phenomena*; Domb, C., Lebowitz, J., Eds.; Academic: London, 1990.
- (80) Garland, C. W. *Liquid Crystals: experimental study of physical properties and phase transitions*; Kumar, S., Ed.; Cambridge University Press: New York, 2001; Chapter 7.
- (81) Chirtoc, M.; Hadj Sahraoui, A.; Kolinsky, C.; Buisine, J. M. *Rev. Sci. Instrum.* **2002**, *73*, 2773–2780.
- (82) [http://www.engineeringtoolbox.com/water-thermal-properties-d\\_162.html](http://www.engineeringtoolbox.com/water-thermal-properties-d_162.html) (accessed October 1, 2008).